CHEMISTRY OF MATERIALS

Article

pubs.acs.org/cm

Molecular Engineering Design to Resolve the Layering Habit and Polymorphism Problems in Deep UV NLO Crystals: New Structures in $MM'Be_2B_2O_6F$ (M=Na, M′=Ca; M= K, M′=Ca, Sr)

Hongwei Huang,[†,‡] Jiyong Yao,[†] Zheshuai Lin,[†] Xiaoyang Wang,[†] Ran He,[†,‡] Wenjiao Yao,[†,‡] Naixia Zhai,[†,‡] and Chuangtian Chen*[,†]

[†]Center for Crystal Research and Development, Technical Institute of Physics and Chemistry, Chinese Academy of Sciences, Beijing 100190, China

[‡]Graduate University of the Chinese Academy of Sciences, Beijing 100049, China

Supporting Information

ABSTRACT: A novel series of alkali and alkaline earth metal combined fluorine beryllium borates $NaCaBe_2B_2O_6F$, $KCaBe_2B_2O_6F$, and $KSrBe_2B_2O_6F$ were successfully synthesized through molecular engineering design and grown in crystals by spontaneous nucleation technique from self-flux systems. The idea, introduction of relatively small alkali and alkaline earth metal cations and the fluorine anion, successfully resulted in the novel UV NLO crystal $NaCaBe_2B_2O_6F$, the following substitution of cations directed to two centrosymmetric compounds $KCaBe_2B_2O_6F$ and $KSrBe_2B_2O_6F$. In all of their structures, the $a-b$ plane is the infinite lattice layer $(Be_3B_3O_6F_3)_\infty$ made up of BO_3 and BeO_3F anionic groups, and for the first time, it was found that the adjacent layers are connected with fluorine bridge atoms to form $(Be_6B_6O_{12}F_3)_\infty$ double layers, instead of oxygen bridge atoms usually occurred in other oxides. This structural characteristic is greatly beneficial to improve the layering-growth habit and eliminate polymorphism of a crystal. Optical measurements on the nonlinear optical crystal of $NaCaBe_2B_2O_6F$ reveal that this crystal is phase-matchable and its short-wavelength absorption edge is down to deep UV (below 190 nm). Theoretical calculations on electronic structure were carried out to explain the experimental results. Our preliminary results indicate that $NaCaBe_2B_2O_6F$ has promising applications in the UV spectrum region.

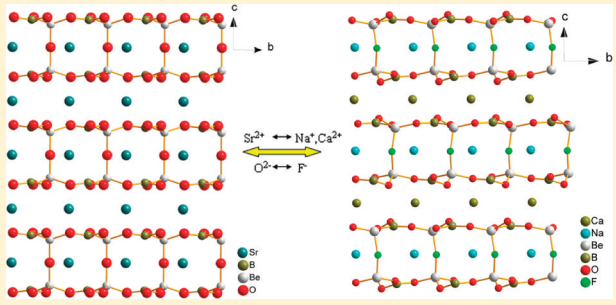

KEYWORDS: *fluorine beryllium borates, nonlinear optical crystal, deep uv, crystal growth*

INTRODUCTION

Deep ultraviolet (UV) nonlinear optical (NLO) materials that can produce deep UV coherent light (λ< 200 nm) are of great importance owing to their promising applications in many advanced technology areas, such as semiconductor photolithography, laser micromachining, photochemical synthesis, as well as superhigh-resolution and angle-resolved photoemission spectrometers.[1,2] Concentrated researches in this area especially for noncentrosymmetric materials have been made for decades.[3,4] The anionic group theory,[5−7] which reveals that the NLO properties of crystal are dominantly determined by the anionic groups, has been very successful in developing ultraviolet (UV) and deep UV NLO crystals in borates. Over years several important UV NLO crystals have been discovered, including β-BaB_2O_4 (BBO),[8] LiB_3O_5 (LBO),[9] CsB_3O_5 (CBO),[10] $CsLiB_6O_{10}$ (CLBO),[11,12] and $YCa_4O(BO_3)_3$ (YCOB),[13] which have been widely used in NLO optics. Nowadays, the search for new NLO materials, particularly for deep UV applications, has attracted considerable attention.[14−20]

The exploring of new deep UV NLO crystals is limited to the alkali and alkaline-earth metal because it should be transparent to the radiation wavelength as short as possible. In particular, the $[BO_3]$ group has been recognized as the basic structural unit to search for the deep UV NLO crystals since this planar anionic group would possess a relatively larger anisotropic response to the incident radiation. Recently, a great breakthrough in deep UV NLO crystals is the discovery of the $KBe_2BO_3F_2$[21−23] crystal and its significant applications in the modern instruments such as the laser ultrahigh-resolution photoemission spectroscopies.[1,2] The excellent NLO properties of KBBF crystal including relatively large SHG coefficient, a short absorption edge and moderate birefringence are mainly determined by the $(Be_2BO_3F_2)_\infty$ layer made up of the trigonal planar $[BO_3]$ unit and the tetrahedral $[BeO_3F]$ unit. However, since there is no bonding between the adjacent layers, the KBBF crystal is very difficult to grow in thickness because of its strong layer tendency, which severely limits the power of coherent laser output.

Received: September 24, 2011
Revised: November 7, 2011
Published: November 17, 2011

To overcome the crystal-growth problems and keep all of the brilliant optical properties in the KBBF crystal, our group designed and synthesized $Sr_2Be_2B_2O_7$ (SBBO) by the molecular engineering method.[24] In the structure of SBBO, BeO_4 tetrahedrons and planar BO_3 triangles are alternately arranged in a trigonal pattern and connected via common O corners to generate a nearly planar infinite $[Be_3B_3O_6]_\infty$ network perpendicular to the *c* axis, which provide large SHG coefficients and sufficient birefringence. The binding between the $[Be_3B_3O_6]$ layers is stronger, as they are bridged by O atoms bound to Be atoms. Therefore, this spacial arrangement shares all of the favorable NLO properties of KBBF, and is responsible for the weaker layer habit and conducive to bulk crystals growth. Unfortunately, the fine structure of SBBO has not been solved yet (the structural convergence index >0.065[24]) because of the structural polymorphism problem, which is very likely resulted from the markedly longer bond length between Be and the bridged O that leads to the stacking fault and twinning of the adjacent $[Be_3B_3O_6]$ layers.[25] So there is great demand for developing the new structure that can overcome the structural disadvantages in KBBF and SBBO, while possessing the comparable SHG capability in the deep UV spectral region.

It is well-known that the electrostatic interactions between ions are proportional to charges and inversely proportional to square of radius. Thus, small alkali or alkaline earth metal will be beneficial to reinforce the electrostatic force between cations and anionic frameworks which will in turn relieve the layering habit to some extent. On the other hand, the shorter and stronger interactions caused by smaller cations can draw the NLO-active anionic groups closer to each other forming a denser packing to produce larger NLO effects. Besides, we utilized F^- as partial substitution of O^{2-} in SBBO for the following reasons: first the incorporation of the fluorine element can effectively cause the UV absorption edge of a crystal blue-shift, second the relatively longer Be−F bond may be good for eliminating structural polymorphism, third the mutual assemblage of more elements into a compound is likely to isolate new phases with interesting stoichiometries, structures and properties. Guided by this idea, we successfully obtained the novel UV NLO crystal $NaCaBe_2B_2O_6F$. Afterward, our attempt of cation substitution experiments directed to the appearance of $KCaBe_2B_2O_6F$ and $KSrBe_2B_2O_6F$. Although the latter two crystallize in centrosymmetric structures, they further illuminate the influence of the size and charge of cations on the packing of anionic frameworks. All of these structures consist of the same infinite lattice $(Be_6B_6O_{12}F_3)_\infty$ double layers, which were connected by bridged F atoms in stead of bridged O atoms in SBBO. This structural feature is greatly helpful to improve the layering-growth habit and eliminate polymorphism (e.g., layer-twinning) of a crystal. Moreover, $NaCaBe_2B_2O_6F$ has been found to be a phase-matchable NLO crystal and its short-wavelength absorption edge is down to below 190 nm. In addition, the syntheses, crystal growth, structure, linear and NLO properties, thermal behaviors of these crystals were performed. Our preliminary results indicate that $NaCaBe_2B_2O_6F$ may have potential application in UV range.

EXPERIMENTAL SECTION

Synthesis. $CaCO_3$ (AR), $SrCO_3$ (AR), BeO (99.5%), B_2O_3 (99.5%), NaF(AR), KF (AR), CaF_2 (AR) and SrF_2 (99%) from commercial sources were used as received. Polycrystalline samples for $NaCaBe_2B_2O_6F$, $KCaBe_2B_2O_6F$ and $KSrBe_2B_2O_6F$ were prepared by high-temperature solid state reaction. The raw materials were mixed in stoichiometric proportions, then were gradually elevated to sintering temperatures of 710, 730, and 740 °C respectively and kept at this temperature in air for 48 h. The powder samples were characterized by powder X-ray diffraction. Because of the toxicity of BeO, all of the experiments were performed in a ventilated system.

Crystal Growth. All of the crystals have been grown successfully from B_2O_3-MF-M′F_2 (M═Na, K; M′═Ca, Sr) flux system, and the spontaneous crystallization technique was used. The $NaCaBe_2B_2O_6F$ single crystal was grown with B_2O_3−NaF-CaF_2 serving as flux. A mixture (50 g) of $NaCaBe_2B_2O_6F$ powder with B_2O_3, NaF, and CaF_2 at the molar ratio of 1:1:4.7:0.5 was thoroughly ground and put into a platinum crucible and then gradually heated up to 850 °C in a programmable temperature electric furnace. It was held at this temperature for 48 h and stirred to ensure complete dissolution of the solute and mixes homogeneously. Afterward, the temperature was lowered to the saturation temperature (720 °C) in a day and decreased at a rate of 1 °C/day. When the growth of crystal was completed, it was lifted out of the liquid surface by a platinum wire, the temperature of the furnace was then reduced to room temperature within 2 days. Successfully a $NaCaBe_2B_2O_6F$ single crystal with dimensions of 30 × 30 × 4 mm^3 was obtained (see Figure S1 in the Supporting Information).

Similarly, single crystals of $KCaBe_2B_2O_6F$ and $KSrBe_2B_2O_6F$ were also obtained from their self-flux systems by spontaneous crystallization. The flux proportions of two crystals (B_2O_3−KF-CaF_2, B_2O_3−KF-SrF_2) are the same as that of $NaCaBe_2B_2O_6F$. The small single crystals were obtained by dissolving the flux attached to the crystals in boiling water (see Figure S1 in the Supporting Information).

Structure Determination. Single-crystal X-ray diffraction data were collected with the use of graphite-monochromatized Mo K_α (λ = 0.71073 Å) at 293 K on a Rigaku AFC10 diffractometer equipped with a Saturn CCD detector. Crystal decay was monitored by recollecting 50 initial frames at the end of data collection and no detectable crystal decay was observed. The collection of the intensity data was carried out with the program Crystalclear.[26] Cell refinement and data reduction were carried out with the use of the program Crystalclear[26] and face-indexed absorption correction was performed numerically with the use of the program XPREP.[26]

The structure was solved with Direct Methods implemented in the program SHELXS and refined with the least-squares program SHELXL of the SHELXTL.PC suite of programs.[27] The $NaCaBe_2B_2O_6F$ crystal was a racemic merohedral twin with fractional contributions of domains being 0.26, 0.33, 0.29, and 0.12. The final refinement included anisotropic displacement parameters. The program STRUCTURE TIDY[28] was then employed to standardize the atomic coordinates. Additional details and structural data are given in Table 1 and further information may be found in the Supporting Information (Tables S1−S3).

Powder X-ray Diffraction. X-ray powder diffraction patterns of polycrystalline samples were recorded on a Bruker D8 ADVANCE X-ray diffractometer with Cu Kα radiation (λ = 1.5418 Å). The scanning step width of 0.02° and the scanning rate of 0.2° s^{-1} were applied to record the patterns in the 2θ range of 10−75°. The experimental X-ray powder diffraction pattern of sample and the theoretical simulation from the single-crystal crystallographic data are in good accordance (Figure S2 in the Supporting Information).

Element Analysis. A Varian 710-ES (USA, Varian) inductively coupled p10lasma optical emission spectrometer (ICP-OES) with Sepex Certiprep standards was employed to analyze the elements of the crystal. The crystal samples were dissolved in nitric acid (5 mL) at the boiling point for 1 h.

Thermal Analysis. The thermal properties of title compounds were investigated by differential scanning calorimetric (DSC) analysis using the Labsys TG-DTA16 (SETARAM) thermal analyzer (the DSC was calibrated with Al_2O_3). A 10 mg powder sample of crystals was placed in a platinum crucible and heated from room temperature to 1250 °C at a rate of 10 °C/min in nitrogen atmosphere. The melted

Table 1. Crystal Data and Structure Refinement for $NaCaBe_2B_2O_6F$, $KCaBe_2B_2O_6F$, and $KSrBe_2B_2O_6F$

formula	$NaCaBe_2B_2O_6F$	$KCaBe_2B_2O_6F$	$KSrBe_2B_2O_6F$
fw	217.71	233.82	281.36
cryst syst	monoclinic	trigonal	hexagonal
space group	*Cc*	$P\bar{3}1c$	$P6_3/m$
a (Å)	4.6232(9)	4.7054(16)	4.7652(10)
b (Å)	8.008(3)	4.7054(16)	4.7652(10)
c (Å)	14.182(3)	14.554(3)	15.050(3)
α (deg)	90.00	90.00	90.00
β (deg)	90.00(3)	90.00	90.00
γ (deg)	90.00	120.00	120.00
V (Å3)	525.1(2)	279.07(15)	295.96(11)
Z	4	2	2
cryst size (mm^3)	0.3 × 0.23 × 0.17	0.3 × 0.2 × 0.15	0.15 × 0.13 × 0.08
ρ(calcd) (g/cm^3)	2.754	2.783	3.157
T (K)	293(2)	293(2)	293(2)
λ (Å)	0.71073	0.71073	0.71073
F(000)	424	228	264
μ (mm^{-1})	1.275	1.869	9.810
θ (deg)	4.31−32.53	5.00−29.98	4.94−32.57
index range	$-6 \le h \le 6$	$-6 \le h \le 6$	$-7 \le h \le 6$
	$-10 \le k \le 12$	$-6 \le k \le 6$	$-7 \le k \le 7$
	$-21 \le l \le 20$	$-20 \le l \le 20$	$-22 \le l \le 22$
R_{int}	0.0482	0.0252	0.0405
measured reflns	2699	3409	3752
independent reflns	1584	283	376
reflns with $I > 2\sigma(I)$	1315	267	324
data/restraints/params	1584/2/54	283/0/22	376/0/22
$R(F)$ for $F_o^2 > 2\sigma(F_o^2)^a$	0.0604	0.0193	0.0302
$wR\ (F_o^2)^b$	0.1304	0.0666	0.0603
GOF on F^2	0.999	1.090	2.203
largest diff. peak and hole (e $Å^{-3}$)	0.922 and −0.770	0.265 and −0.406	0.925 and-0.596

$^aR(F) = \sum||F_o| - |F_c||/\sum|F_o|$ for $F_o^2 > 2\sigma(F_o^2)$. $^bR_w(F_o^2) = \{\sum[w(F_o^2 - F_c^2)^2]/\sum wF_o^4\}^{1/2}$ for all data.

residues were examined and analyzed by X-ray powder diffraction after the experiments.

Second-Harmonic Generation. Second-harmonic generation (SHG) test was performed on ground crystals of $NaCaBe_2B_2O_6F$ by means of the Kurtz-Perry method.[29] The sample was irradiated with a pulsed infrared beam (10 ns, 3 mJ, 10 kHz) produced by a Q-switched Nd:YAG laser at wavelength of 1064 nm. As powder SHG effect depends strongly on the particle size, $NaCaBe_2B_2O_6F$ crystals were ground and sieved into the following particle size ranges: 35−50, 50−74, 74−105, 105−150, and 150−200 μm, respectively. Microcrystalline KH_2PO_4 (KDP) samples within the corresponding size ranges served as the standard.

UV Transmittance Spectroscopy. The UV optical transmittance spectrum was measured at room temperature using a spectrophotometer (VUVas2000, McPherson) in the wavelength range from 120 to 380 nm.

First-Principles Calculations. The electronic structures, as well as the linear and nonlinear optical properties, of the $NaCaBe_2B_2O_6F$ crystal were obtained by the plane-wave pseudopotential method,[30,31] which has been successfully applied on many borate NLO crystals.[32] The optimized norm-conserving pseudopotentials[33] in the Kleinman-Bylander form[34] for Na, Ca, Be, B, O, and F are used to ensure a small plane-wave basis set without compromising the accuracy. Local density approximation (LDA) with a very high kinetic energy cutoff of 900 eV is adopted. Monkhorst−Pack *k*-point meshes[33] with a density of (2 × 2 × 2) points in the Brillouin zone of the $NaCaBe_2B_2O_6F$ unit cell are chosen. Tests show that the total energy with the above computational parameters is accurate to 15 meV/atom, which is adequate for the current studies.

RESULTS AND DISCUSSION

Structure of $NaCaBe_2B_2O_6F$. $NaCaBe_2B_2O_6F$ crystallizes into the noncentrosymmetric monoclinic space group *Cc*, the crystal structure is illustrated in Figure 1. The B atom is bound

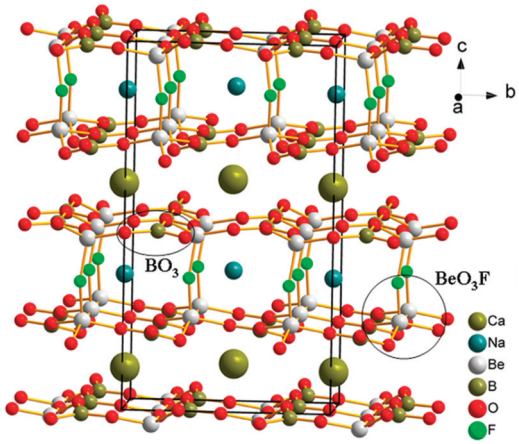

Figure 1. Crystal structure of $NCaBe_2B_2O_6F$.

to three O atoms to form a planar BO_3 with B−O bond length varying from 1.346(10) to 1.385(11) Å and O−B−O bond angles from 116.0(9) to 125.8(7)°. The Be atom coordinated to three O atoms and one F atom are found to be a BeO_3F tetrahedron with the distance of Be−O and Be−F ranging from 1.562(15) to 1.623(12) Å and 1.598(12) to 1.681(11) Å, respectively. Three BO_3 triangles and three BeO_3F tetrahedrons are alternately arranged in a trigonal pattern and connected by sharing bridging O corners to generate a two-dimensional infinite $(Be_3B_3O_6F_3)_\infty$ layer shown in Figure 2. In particular,

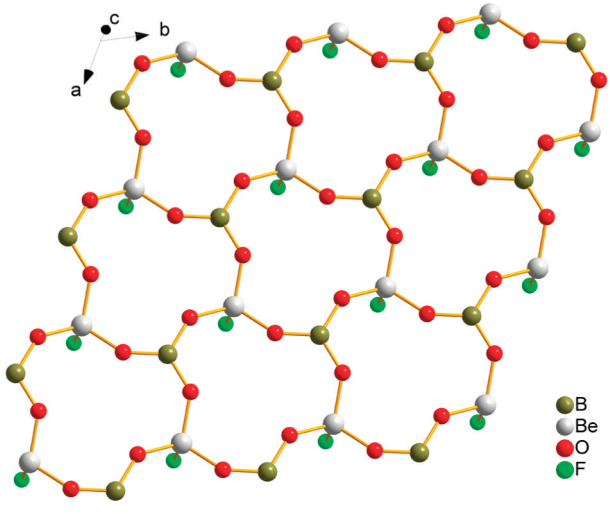

Figure 2. Infinite layers of $(Be_3B_3O_6F_3)_\infty$ in the $NCaBe_2B_2O_6F$ structure.

One $(Be_3B_3O_6F_3)_\infty$ layer links up with another adjacent one reversely through bridging fluorine atoms forming a unique $(Be_6B_6O_{12}F_3)_\infty$ double layers, resulting in a series of tunnels along [010] or [100] direction, Na^+ cations reside in the channels and Ca^{2+} cations are located in the space between two

dx.doi.org/10.1021/cm202870q | *Chem. Mater.* 2011, 23, 5457−5463

neighboring $(Be_6B_6O_{12}F_3)_\infty$ double layers. In the structure of $NaCaBe_2B_2O_6F$, all the $[BO_3]$ groups (NLO-active groups) are slightly deviated from $a-b$ plane and aligned in the different orientation.

Structure of $KCaBe_2B_2O_6F$. $KCaBe_2B_2O_6F$ crystallizes in the centrosymmetric trigonal space group $P\bar{3}1c$, the crystal structure is shown in Figure 3. The B atom is bound to three O

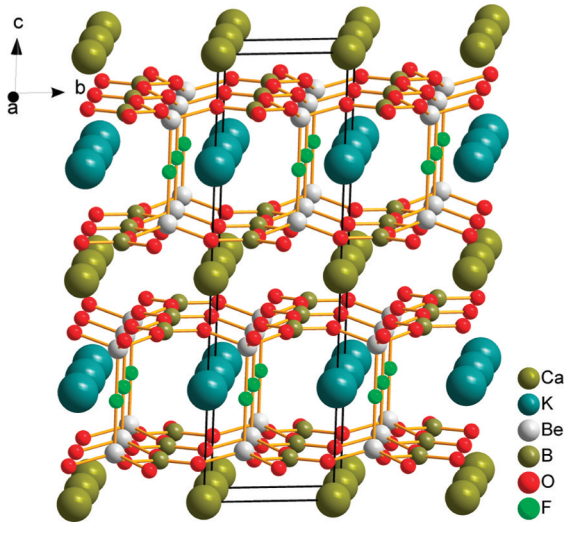

Figure 3. Crystal structure of $KCaBe_2B_2O_6F$.

atoms to form a planar BO_3 and all the B−O bonds share the same length 1.3757(8) Å with O−B−O bond angles ranging from 119.979(5) to 119.980(5)°. The Be atom are coordinated to three O atoms and one F atom to form a BeO_3F tetrahedron with the Be−O bond length of 1.6004(11) and Be−F bond length of 1.697(2) Å. Similarly, the basic building frameworks of $KCaBe_2B_2O_6F$ are also $(Be_6B_6O_{12}F_3)_\infty$ double layers, which was found in the structure of $NaCaBe_2B_2O_6F$ as described above, and the K^+ cations reside in the channels as Na^+ above. In the structure of $KCaBe_2B_2O_6F$, the $[BO_3]$ groups are parallel to $a-b$ plane but aligned in the different orientation.

Structure of $KSrBe_2B_2O_6F$. $KSrBe_2B_2O_6F$ belongs to centrosymmetric Hexagonal system and crystallizes in P63/m space group, the crystal structure is depicted in Figure 4. The B atom is bound to three O atoms to build BO_3 group with B−O bond length of 1.3805(17) Å and the three O−B−O bond angles are equal to 119.94(2)°. The Be atom is coordinated to three O atoms and one F atom to form a BeO_3F tetrahedron with the Be−O bond distance of 1.595(2) Å and Be−F bond distance of 1.673(6) Å, respectively. Though $KSrBe_2B_2O_6F$ also takes the basic building $(Be_6B_6O_{12}F_3)_\infty$ double layers as basic building frameworks, which was discussed in the structure of $NaCaBe_2B_2O_6F$ and $KCaBe_2B_2O_6F$. In the structure of $KSrBe_2B_2O_6F$, all the $[BO_3]$ groups not only parallel to $a-b$ plane but also aligned in the exactly same orientation in the same double layers expecting to give a large NLO contribution. Unfortunately, the centrosymmetric arrangement of NLO-active groups resulted in the cancellation of NLO effect.

The bond valence sums (BVS)[35] of each atom in $NaCaBe_2B_2O_6F$, $KCaBe_2B_2O_6F$ and $KSrBe_2B_2O_6F$ were calculated and listed in the Supporting Information (Tables S4−S6). These results agree with expected oxidation states.

Molecular Engineering Design and Structural Relationship. In our structural design experiments, the following

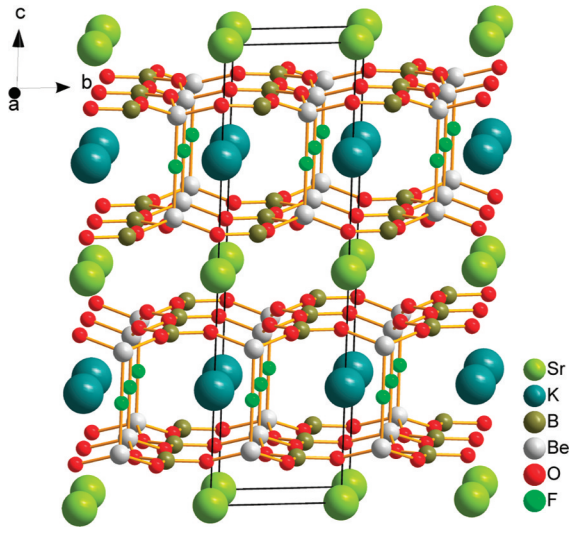

Figure 4. Crystal structure of $KSrBe_2B_2O_6F$.

molecular engineering considerations have been successfully fulfilled. (1) the F atoms are used to substitute the bridge O atoms to improve the bonds between Be and bridged atoms. It is known that the covalence of Be−F bond is lower than that of Be−O bond, and normally the former bond length (~1.69 Å) is larger than the latter (~1.60 Å). This would make the space between the adjacent layers more flexible. So the Be atoms are more "comfortable" to accommodate at their original sites, which decrease the occurrence of stacking fault in crystal. (2) relatively small alkali and alkaline earth metals are employed as cations in order to reinforce the electrostatic interactions, to relieve serious layering habit and increase the density of NLO-active anionic groups. Meanwhile, the including of alkali atoms is able to neutralize the charge modification due to F substitution, while keeping the favorable structural features in KBBF and SBBO. Indeed, all three of the crystals have the same two-dimensional infinite $(Be_3B_3O_6)_\infty$ network composed of BO_3 and BeO_3F, similar to the structure along the $a-b$ plane in KBBF. Two neighboring layers of $(Be_3B_3O_6)_\infty$ network are connected by bridged F atoms, analogy to SBBO, generating a $(Be_6B_6O_{12}F_3)_\infty$ double-layer structure. The alkali metal atoms are located at the tunnels inside the double layers and alkaline earth metal atoms reside in the interstices between the double layers. The structural comparison for the example of SBBO and $NaCaBe_2B_2O_6F$ is shown in Figure 5. The new structural features overcome the polymorphism problem inherent in the structure of SBBO; the structural converge factors for these three crystals are 0.0546 ($NaCaBe_2B_2O_6F$), 0.0193 ($KCaBe_2B_2O_6F$), and 0.0302 ($KSrBe_2B_2O_6F$), much smaller than that of SBBO (>0.065). Meanwhile, the serious layering habit present in KBBF is also greatly improved; our preliminary crystal growth attempts have obtained the crystals with a thickness of more than 3 mm.

On the other hand, it is interesting that the arrangement of anionic groups (mainly BO_3 units) becomes more and more regular, as the cations become bigger, which resulted in the structural evolution from $NaCaBe_2B_2O_6F$, $KCaBe_2B_2O_6F$ to $KSrBe_2B_2O_6F$ (shown in Figure 6). As the charges and radius of metal cations become bigger, the symmetry of crystal structures intends to be higher in this system, shown in Table 2. In our series, only the Na^+ and Ca^{2+} cations are incorporated into the lattice, a UV NLO compound in structure analogous to SBBO

dx.doi.org/10.1021/cm202870q | Chem. Mater. 2011, 23, 5457−5463

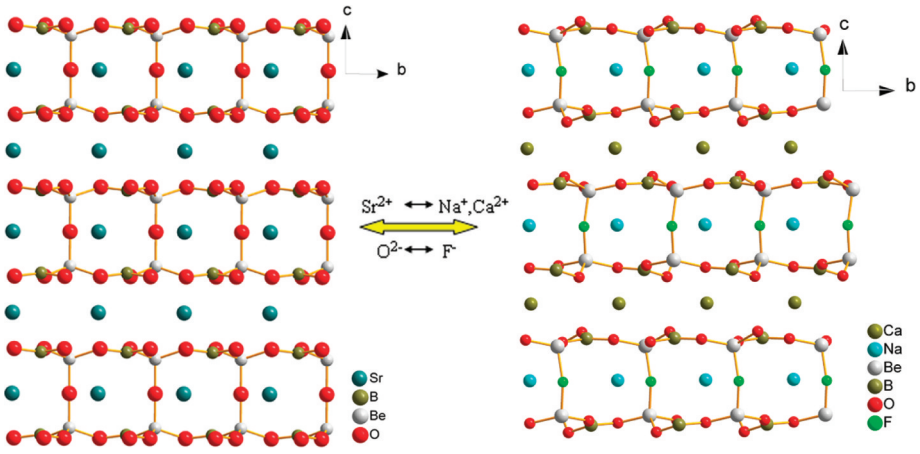

Figure 5. Structure relationship between SBBO and $NaCaBe_2B_2O_6F$.

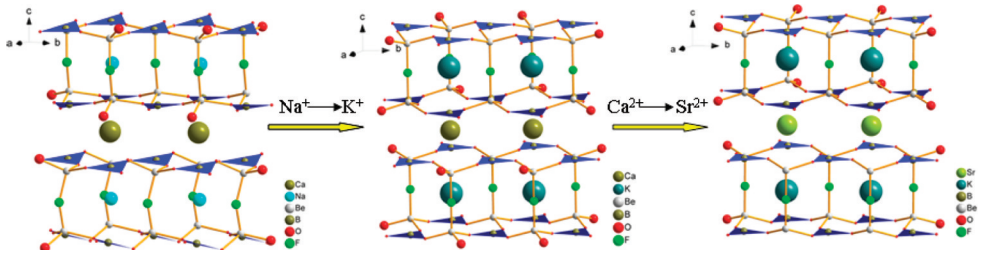

Figure 6. Structural evolution from $NaCaBe_2B_2O_6F$ to $KCaBe_2B_2O_6F$ and $KSrBe_2B_2O_6F$ in the $(Be_6B_6O_{12}F_3)_\infty$ double layers (blue triangles represent BO_3 units).

Table 2. Comparison of the Symmetry of Crystal Structures for the Studied Crystals

crystal	cation	point group	space group	no. of space group
$NaCaBe_2B_2O_6F$	Ca^{2+}, Na^+	*m*	*Cc*	91
KBBF	K^+	32	*R*32	155
$KCaBe_2B_2O_6F$	Ca^{2+}, K^+	$\bar{3}m$	$P\bar{3}1c$	163
$KSrBe_2B_2O_6F$	Sr^{2+}, K^+	6/*m*	$P6\bar{3}/m$	176
SBBO	Sr^{2+}	$\bar{6}m2$	$P\bar{6}c2$	188

without structural polymorphism was successfully created. The proper combination of alkali and alkaline earth metal cations with the bridged F configuration is suitable to produce the good NLO effects without having serious layering habit and the polymorphism problem in these SBBO-like crystals. This may provide a new path to search for the deep UV NLO crystals. The relevant studies are in progress.

UV Transmittance Spectroscopy. The UV optical transmittance spectrum of $NaCaBe_2B_2O_6F$ crystal was recorded at room temperature on a crystal in the size of 5 × 2.5 × 1 mm^3 and polished on both sides. As shown in Figure 7, the UV short-wavelength absorption edge of $NaCaBe_2B_2O_6F$ is located at 190 nm, which is comparable to that of the universally used crystals BBO (189 nm), indicating that the crystal may have potential prospects in UV NLO application. Obviously, our transmittance spectrum measurement on single crystal gives more accurate results than the powder diffuse reflectance method.

Nonlinear Optical Properties. Because of the noncentrosymmetric crystal structure of $NaCaBe_2B_2O_6F$, it is expected to possess NLO properties. The curves of the powder SHG signals as a function of particle size were detected and

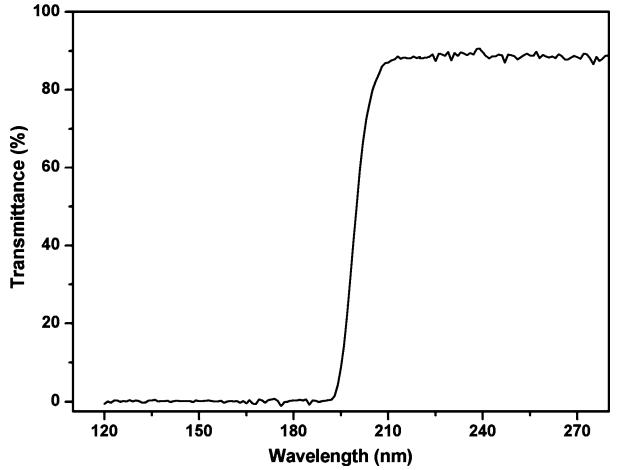

Figure 7. Transmittance of $NaCaBe_2B_2O_6F$ crystal in the UV region.

compared with that of KDP (Figure 8). It was consistent with the phase-matching behavior according to the rule proposed by Kurtz and Perry.[28] According to the anionic group theory of NLO activity in borates, the BO_3 trigonal planes are responsible for the large SHG effects, and also, the different orientations of the structure limit their total NLO contribution. In the structure of $NaCaBe_2B_2O_6F$, the arrangement of $[BO_3]$ groups is in an unfavorable manner so that the resulting SHG effects are limited. Consequently, the second-harmonic signal of $NaCaBe_2B_2O_6F$ was found to be about 1/3 times as large as that of KDP standard.

Thermal Behavior. Differential scanning calorimetric (DSC) measurements were carried out with ground crystals of title compounds (see the Supporting Information). All the

dx.doi.org/10.1021/cm202870q | *Chem. Mater.* 2011, 23, 5457–5463

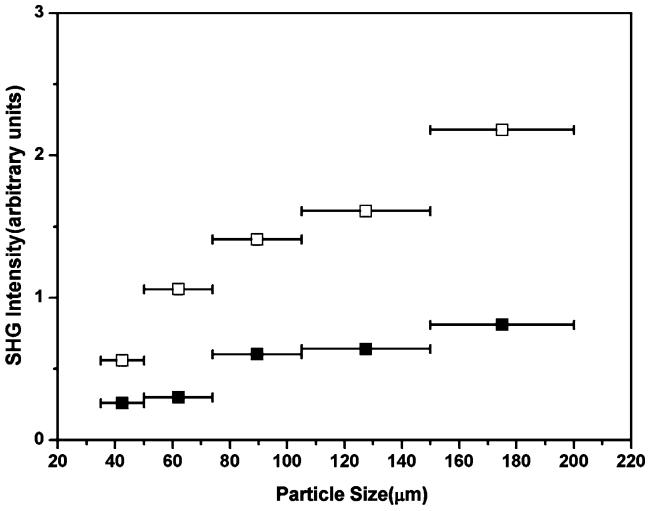

Figure 8. SHG measurements of $NaCaBe_2B_2O_6F$ ground crystals (■) with KDP (□) as a reference.

DSC curves exhibit one endothermic peak on the heating curves at 890, 920, and 925 °C, respectively. The XRD patterns of melted residues, which mainly displayed BeO peak, were clearly different from that of original crystals. The results demonstrate the title compounds all melts incongruently. Therefore, they must be grown under the melting temperature by flux methods.

Element Analysis. The results of ICP elemental analysis listed in Table S7 corresponded to the proportions determined from single-crystal X-ray analysis.

Theoretical Calculations. The partial density of state (PDOS) for $NaCaBe_2B_2O_6F$ is shown in Figure S4, in which only the upper region of the valence band (VB) and the bottom of conduction band (CB) are shown, since the optical properties of a crystal in the visible and UV spectrum are mainly determined by the states close to the band gap.[36] It is clear that in these states the contribution from the orbitals of the alkali and alkaline earth metal cations is negligibly small, despite that the orbitals of the cations with larger size becomes slightly significant at the bottom of CB. Meanwhile, the Be orbitals also have very little contributions to the states close to the band gap, and the F orbital are distributed below 2.5 eV from the VB maximum. The VB maximum and CB minimum are composed of the O 2p and B 2p orbitals, respectively, indicating that the optical transition between these states (in the BO_3 groups) indeed determine the main optical properties of the crystal.

Based on the electronic structure, the dispersions of the linear refractive indices for this crystal are calculated, as displayed in Figure S5 in the Supporting Information. $NaCaBe_2B_2O_6F$ is a negative biaxial crystal with the almost equal n_x and n_y. It has moderate birefringence, $\Delta n = 0.057$ at 800 nm. Furthermore, our ab initio calculations reveal that the SHG coefficients for $NaCaBe_2B_2O_6F$ are $d_{31} = -0.22$ pm/V, $d_{22} = -0.15$ pm/V, and $d_{23} = -0.10$ pm/V, approximately one-half as large as that of KDP. The calculated values are consistent with the experimental measurements.

These optical properties can be elucidated from the microscopic structural features of $NaCaBe_2B_2O_6F$ crystal, shown as follows: According to the anionic group theory, in the alkali and alkaline-earth borate crystals the B−O groups are the dominating active microscopic units which determine the birefringence and SHG coefficient.[32] In $NaCaBe_2B_2O_6F$, all of the $[BO_3]$ groups are nearly in the same plane normal to the *c*-axis with the dihedral angles less than 15° (see Figure4). So its anisotropic responds to the incident light is moderate ($\Delta n \sim 0.06$). By comparison, the perfect in-plane (BO_3) arrangement could result in larger birefringence about 0.08 as in the case of KBBF.[37] However, the $[BO_3]$ groups, the main active units responsible for the SHG effects as well, are some antialigned to those in the neighbor a-b planes (see Figure1). Therefore, the microscopic second-order susceptibilities of $[BO_3]$ groups are partly canceled, which makes the SHG coefficients of $NaCaBe_2B_2O_6F$ relatively small.

■ CONCLUSIONS

A new category of alkali and alkaline earth metal combined fluorine beryllium borates $NaCaBe_2B_2O_6F$, $KCaBe_2B_2O_6F$ and $KSrBe_2B_2O_6F$ have been obtained through structural design. The title compounds were all grown in crystals from their self-flux systems by spontaneous crystallization. Introduction of relatively small cations Na^+ and Ca^{2+} with the incorporation of F^- starting from the structure of $Sr_2Be_2B_2O_7$ successfully led to the finding of the novel UV NLO crystal $NaCaBe_2B_2O_6F$. The cations replacement of K^+ for Na^+ and Sr^{2+} for Ca^{2+} directed to the appearance of centrosymmetric $KCaBe_2B_2O_6F$ and $KSrBe_2B_2O_6F$. For the first time, they were found crystallizing in structures consisting of $(Be_6B_6O_{12}F_3)_\infty$ double layers bridged by F atoms, meanwhile overcoming structural polymorphism (layer-twinning) and serious layering growth habit present in SBBO and KBBF, respectively, which was confirmed by our experiments. Second-harmonic generation (SHG) measurement on ground $NaCaBe_2B_2O_6F$ crystals reveals it is a phase-matchable NLO crystal and the short-wavelength absorption edge is down to 190 nm. According to theoretical calculations on electronic structure, the BO_3 groups determine the main optical properties of the crystal. Our preliminary results indicate that $NaCaBe_2B_2O_6F$ may be a promising UV NLO crystal. We believe the molecular engineering procedures present in this work would provide a new path to search for the deep UV NLO crystals.

■ ASSOCIATED CONTENT

Ⓢ Supporting Information

DSC traces, crystal pictures, X-ray powder diffraction patterns, and crystal data (CIF) for $NaCaBe_2B_2O_6F$, $KCaBe_2B_2O_6F$, and $KSrBe_2B_2O_6F$. This material is available free of charge via the Internet at http://pubs.acs.org.

■ AUTHOR INFORMATION

Corresponding Author

*Tel.: +86-10-82543705. Fax: +86-10-82543709. E-mail: cct@mail.ipc.ac.cn..

■ ACKNOWLEDGMENTS

This work was supported by the National Natural Science Foundation of China under Grants 50590402, and 91022036, and the National Basic Research Project of China (2010CB630701, and 2011CB922204).

■ REFERENCES

(1) Kiss, T.; Kanetaka, F.; Yokoya, T.; Shimojima, T.; Kanai, K.; Shin, S.; Onuki, Y.; Togashi, T.; Zhang, C.; Chen, C. T.; Watanabe, S. *Phys. Rev. Lett.* **2005**, *94*, 057001.

(2) Koralek, J. D.; Douglas, J. F.; Plumb, N. C.; Griffith, J. D.; Cundiff, S. T.; Kapteyn, H. C.; Murnane, M. M.; Dessau, D. S. *Phys. Rev. Lett.* **2006**, *96*, 017005.
(3) Halasyamani, P. S.; Poeppelmeier, K. R. *Chem. Mater.* **1998**, *10*, 2753.
(4) Ok, K. M.; Chi, E. O.; Halasyamani, P. S. *Chem. Soc. Rev.* **2006**, *35*, 710−717.
(5) Chen, C. *Sci. Sin. (Engl. Ed.)* **1979**, *22*, 756.
(6) Chen, C. T.; Liu, G. Z. *Annu. Rev. Mater. Sci.* **1986**, *16*, 203.
(7) Chen, C. T.; Wu, Y. C.; Li, R. K. *Int. ReV. Phys. Chem.* **1989**, *8*, 65.
(8) Chen, C. T.; Wu, B. C.; Jiang, A. D.; You, G. M. *Sci. Sin., Ser. B* **1985**, *28*, 235.
(9) Chen, C. T.; Wu, Y. C.; Jiang, A. D.; Wu, B. C.; You, G. M.; Li, R. K.; Lin, S. J. *J. Opt. Soc. Am. B* **1989**, *6*, 616.
(10) Wu, Y. C.; Sasaki, T.; Nakai, S.; Yokotani, A.; Tang, H. G.; Chen, C. T. *Appl. Phys. Lett.* **1993**, *62*, 2614.
(11) Mori, Y.; Kuroda, I.; Nakajima, S.; Sasaki, T.; Nakai, S. *Appl. Phys. Lett.* **1995**, *67*, 1818.
(12) Tu, J. M.; Keszler, D. A. *Mater. Res. Bull.* **1995**, *30*, 209.
(13) Lei, S.; Huang, Q.; Zheng, Y.; Jiang, A.; Chen, C. *Acta Crystallogr., Sect. C* **1989**, *45*, 1861.
(14) Wang, S. C.; Ye, N.; Li, W.; Zhao, D. *J. Am. Chem. Soc.* **2010**, *132*, 8779.
(15) Zhang, W. L.; Cheng, W. D.; Zhang, H.; Geng, L.; Lin, C. S.; He, Z. Z. *J. Am. Chem. Soc.* **2010**, *132*, 1508.
(16) Wu, H. P.; Pan, S. L.; Poeppelmeier, K. R.; Li, H. Y.; Jia, D. Z.; Chen, Z. H.; Fan, X. Y.; Yang, Y.; Rondinelli, J. M.; Luo, H. S. *J. Am. Chem. Soc.* **2011**, *133*, 7786.
(17) Chen, M. C.; Li, L. H.; Chen, Y. B.; Chen, L. *J. Am. Chem. Soc.* **2011**, *133*, 4617.
(18) Jin, S. F.; Cai, G. M.; Wang, W. Y.; He, M.; Wang, S. C.; Chen, X. L. *Angew. Chem., Int. Ed.* **2010**, *49*, 4967.
(19) Fan, X. Y.; Pan, S. L.; Hou, X. L.; Tian., X. L.; Han, J.; Haag, J.; Poeppelmeier, K. R. *Cryst. Growth Des.* **2010**, *10*, 252.
(20) Huang, H. W.; Yao, J. Y.; Lin, Z. S.; Wang, X. Y.; He, R.; Yao, W. J.; Zhai, N. X.; Chen, C. T. *Angew. Chem., Int. Ed.* **2011**, *50*, 9141.
(21) Chen, C. T.; Xu, Z. Y.; Deng, D. Q.; Zhang, J.; Wong, G. K. L. *Appl. Phys. Lett.* **1996**, *68*, 2930.
(22) Cyranoski, D. *Nature.* **2009**, *457*, 953.
(23) Chen, C. T.; Wang, G. L.; Wang, X. Y.; Xu, Z. Y. *Appl. Phys. B: Laser Opt.* **2009**, *97*, 9.
(24) Chen, C. T.; Wang, Y. B.; Wu, B. C.; Wu, K.; Zeng, W.; Yu, L. H. *Nature.* **1995**, *373*, 322.
(25) Meng, X. Y.; Wen, X. H.; Liu, G. L. *J. Korean Phys. Soc.* **2008**, *52*, 1277.
(26))*CrystalClear*; Rigaku Corp.: Tokyo, 2008.
(27) Sheldrick, G. M. *Acta Crystallogr., Sect. A* **2008**, *64*, 112.
(28) Gelato, L. M.; Parthé, E. *J. Appl. Crystallogr.* **1987**, *20*, 139.
(29) Kurtz, S. K.; Perry, T. T. *J. Appl. Phys.* **1968**, *39*, 3798.
(30) Payne, M. C.; Teter, M. P.; Allan, D. C.; Arias, T. A.; Joannopoulos, J. D. *Rev. Mod. Phys.* **1992**, *64*, 1045.
(31) Clark, S. J.; Segall, M. D.; Pickard, C. J.; Hasnip, P. J.; Probert, M. J.; Refson, K.; Payne, M. C. *Z. Kristallogr.* **2005**, *220*, 567.
(32) Chen, C. T.; Lin, Z. S.; Wang, Z. Z. *Appl. Phys. B: Lasers Opt.* **2005**, *80*, 1.
(33) Lin, J. S.; Qtseish, A.; Paye, M. C.; Heine, V. *Phys. Rev. B* **1993**, *47*, 4174.
(34) Kleinman, L.; Bylander, D. M. *Phys. Rev. Lett.* **1982**, *48*, 1425.
(35) Brown, I. D.; Altermatt, D. *Acta Crystallogr., Sect. B* **1985**, *41*, 24.
(36) Lee, M. H.; Yang, C. H.; Jan, J. H. *Phys. Rev. B* **2004**, *70*, 235110.
(37) Chen, C. T.; Ye, N.; Lin, J.; Jiang, J.; Zeng, W. R.; Wu, B. C. *Adv. Mater.* **1999**, *11*, 1071.